Laser Interferometric Dilatometer Applicable to Temperature Range from 1300 to 2000 K [1]

H. Watanabe,[2, 3] **N. Yamada,**[2] **and M. Okaji**[2]

A laser interferometric dilatometer has been developed for measuring the thermal expansion of high-temperature solids in the temperature range 1300 to 2000 K. The dilatometer consists of a double-path optical heterodyne interferometer, a spectral-band radiation thermometer, and a vacuum chamber with carbon-composite heaters. The performance of the dilatometer has been assessed on the basis of measurements of linear thermal expansion coefficients for glassy carbon. The relative standard deviation of the measured values from those calculated from the fitting polynomial is 0.63 % over the temperature range investigated. The combined standard uncertainties in the measured values are estimated to be less than 1.3 % over this range. The process of sample relocation predominantly affects the reproducibility of the experimental results.

KEY WORDS: dilatometer; glassy carbon; high temperature; optical heterodyne interferometer; pyrometry; thermal expansion.

1. INTRODUCTION

There has been a growing demand for reliable data on the thermal expansion for solids at high temperatures ($T > 1300\ \mathrm{K}$) because of increasing requirements for the accuracy and reliability of operation of the assemblies, machines, and devices available at elevated temperatures. Relative measurement devices such as push-rod dilatometers have generally been used to measure thermal expansion coefficients for solids. Reference materials for thermal expansion measurements are needed for the calibration and testing of these devices. However, there has been a lack of reference materials available at temperatures greater than 1300 K. This is because the National

Institute of Standards and Technology (NIST) no longer supplies the following standard reference materials (SRMs):

SRM 737—tungsten, certified from 80 to 1800 K [1],

SRM 732—sapphire single crystal, certified from 293 to 2000 K [2].

Developments of interferometric dilatometers are indispensable for satisfying the demand for reliable data from the following two points of view: (a) the devices have been used for certifying thermal expansion data for the reference materials, and (b) they are capable of measuring the linear thermal expansion coefficient (α) very precisely in comparison with other absolute measurement techniques. An advantage of the technique for high-temperature measurements is that it can yield expansion data with high precision even for small samples. Using a small sample makes it relatively easy for the temperature distribution within the sample to reach approximate uniformity even at high temperatures.

There have been a few studies [3–5] on developing interferometric dilatometers usable for objects at temperatures greater than 1300 K. In these studies, dc fringe detection methods such as Fizeau interferometry were applied to the interferometric measurements. A disadvantage of such methods is that the uncertainty in the determination of length change depends upon the visibility of fringes, i.e., the magnitudes of the dc signals for fringes. In high-temperature measurements, samples are exposed to elevated temperatures, which lead to some problems associated with losses of mechanical strength, deformations caused by thermal stress, evaporations, and chemical reactions. These problems lead to optical misalignments, causing the dc signal reduction. To minimize such difficulties, Miiller and Cezairliyan have applied a rapid resistive self-heating technique to thermal expansion measurements for Ta [5], Mo [6], and W [7] at high temperatures (~ 3200 K). In these studies, samples were heated to their melting point from room temperature in less than 1 s by the passage of an electrical current pulse through them, and the changes in length and temperature of the sample were measured simultaneously using a Michelson-type interferometer and a high-speed pyrometer, respectively. However, this technique has two shortcomings for high-temperature measurements. The first is the impossibility of application of the technique to nonconducting materials such as ceramics, which are desirable reference materials usable at high temperatures, and the second is the possibility of the drastic increase of temperature differences within a sample resulting from the nonsteady state heating.

One of the other approaches to minimize the problems due to optical misalignments is to use ac fringe detection methods such as optical

heterodyne interferometry, because its performance is remarkably tolerant to a reduction in the dc signal level. The experimental approaches started with the works of Okaji and Imai [8] and Okaji [9], in which values of α for Si in the temperature range of 300 to 1300 K were measured using a dilatometer consisting of a double-path optical heterodyne interferometer, R-type thermocouples, and a radiant image furnace. Accurate data on α for various materials at temperatures below 330 K have been determined using this technique by Okaji et al. [10–14]. The dilatometer can be applied not only to conduction materials, but also to ceramics, and the measurements can be carried out under steady-state conditions. Therefore, it seems suitable for measurements of α for the reference materials available at temperatures greater than 1300 K. The objectives of this study are to describe the dilatometer developed to be used over the temperature range of 1300 to 2000 K and to present experimental results for glassy carbon and the dilatometer's performance. The reason for selecting glassy carbon as the sample is that it is a strong candidate for reference materials for use at high temperatures because of its attractive properties, primarily high chemical durability [15]. In the present study, the influence of sample relocations on reproducibility of the experimental results has been assessed experimentally, because the sample relocation was the main source of uncertainty for measurements with a previous version of the present dilatometer [11].

2. EXPERIMENTAL

2.1. Glassy Carbon Sample

Figure 1 shows a combination of a parallelepiped sample and a reference disc mirror in a sample cell. Laser beams for interferometric measurements run through paths A, A*, B, and B*. The parallelepiped sample, measuring $25 \times 8 \times 6$ mm, was cut out of a disc of glassy carbon. Two (25×8) surfaces of the sample were polished into two parallel optical flats on opposite sides, and changes in thickness between the two surfaces were to be measured. A glassy carbon mirror of 25 mm diameter and 9 mm thickness was placed over the sample. The mirror was used as a reference reflector against the laser beams. A hole with a diameter of 5 mm was drilled through the optical flats of the sample and the mirror for optical pyrometer temperature measurements. Tokai Carbon Co., Ltd. Japan supplied the samples and mirrors, and the material has been designated as GC-20SS. In this study, only one sample was used to evaluate the performance of the dilatometer. The length of the distance between the two optical flats for the sample at 298 K was measured for eight different points
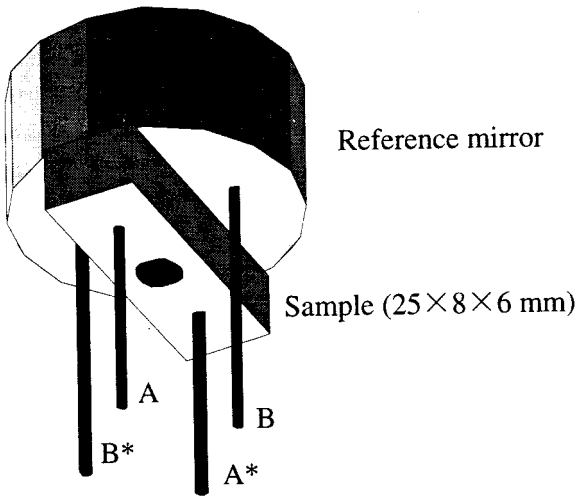
Fig. 1. Schematic diagram of a combination of a parallele-piped sample and a reference disc mirror in a sample cell. Laser beams are running through the paths A, A*, B, and B*.

using a micrometer, and the average value was determined to be 6.033 mm with an uncertainty of 5 μm.

Figure 2 shows a schematic diagram of the cross section of the sample cell containing the combination of sample and mirror. All three components of the cell were made of graphite. There were four holes drilled through the bottom part of the cell where the laser beams passed. One other hole was cut on the bottom part, which had a 5 mm diameter and 8.5 mm depth with a conical bottom. The three holes of the bottom part, sample, and reference mirror were combined into a cylindrical cavity used for optical temperature measurements, as shown in Fig. 2. The size of the cavity was 5 mm in diameter and 23.5 mm in depth, with a conical bottom. The effective emissivity (ε_{cav}) of the cavity was estimated to be 0.998 by using an emissivity value of 0.86 [16] for graphite and the cavity dimensions in the conventional equation [17]. A 5 mm diameter aperture was drilled through the top part of the cell, and the pyrometer was focused on the aperture by observing the image from its viewfinder. To assist in focusing the pyrometer, the conical surface of the top part was fabricated into a multi-leveled form, as shown in Fig. 2. The image of the cell from the viewfinder looks like concentric circles whose center circle corresponds to the aperture. The pyrometer was focused on the aperture as the aperture's image was made in sharp contrast to other circles surrounding it.
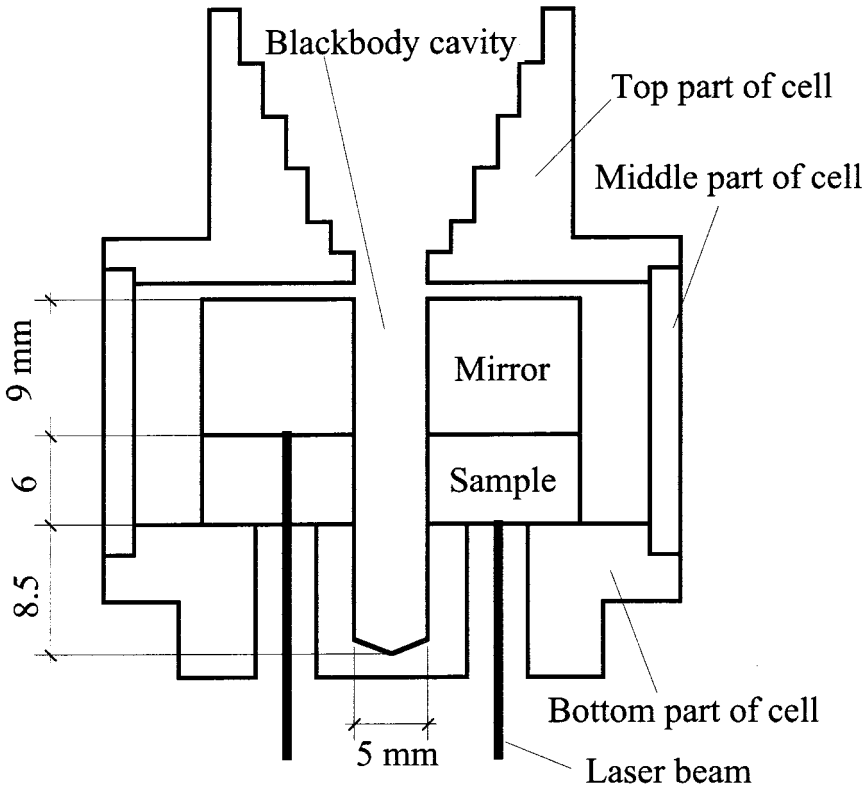
Fig. 2. Schematic diagram of the cross section of the sample cell and combined blackbody cavity. All dimensions are in mm.

2.2. Double-Path Optical Heterodyne Interferometer

Figure 3 shows a schematic diagram of the double-path optical heterodyne interferometer. As the present interferometer is almost the same as that described previously [11], only the main points are described here. The coherent light source for the interferometer is a single-frequency stabilized He–Ne laser (Melles–Griot, Model 05STP901, output power: 1.5 mW). The laser beam is divided into two parallel beams using a combination of a beam splitter (BS1) and a plane reflector (PR) after passing through a half-wave plate (HWP). After that, the two laser beams pass through a couple of acousto-optical modulators (AOM1 and AOM2), which shift the frequencies of the two beams. This method of producing two laser beams having a slight difference in frequency can extinguish the mixing effect between two frequency components in optical heterodyne interferometry
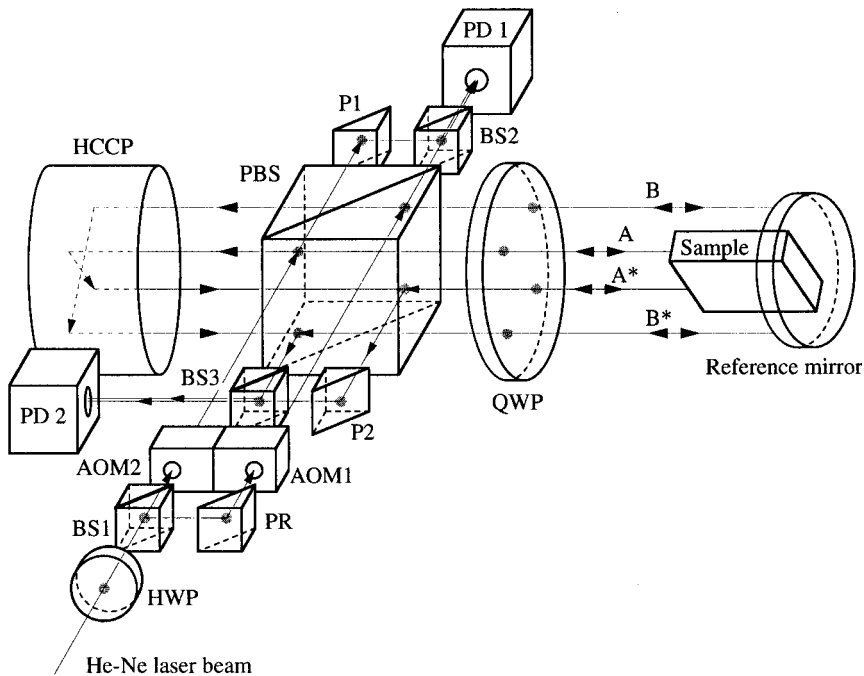
Fig. 3. Schematic diagram of the double-path optical heterodyne interferometer consisting of the following optical elements: acousto-optical modulators AOM1 and AOM2, beam splitters BS1, BS2, and BS3, half-wave plate HWP, hollow cube corner prism HCCP, photodetectors PD1 and PD2, plane reflector PR, polarized beam splitter PBS, prisms P1 and P2, quarter-wave plate QWP.

[11]. After this, either of the two beams is divided into two component beams by a polarized beam splitter (PBS). The two beams polarized parallel to the plane of the interferometer (*p*-polarized) pass through the PBS, and are then introduced into a photodetector (PD1) by a combination of a beam splitter (BS2) and a prism (P1). The other two beams, polarized normal to the plane (*s*-polarized), are reflected by the PBS and introduced into the sample cell after passing through a quarter-wave plate (QWP). As shown in Figs. 1 and 3, the two parallel beams go into the sample cell through paths A and B, and are then reflected by the sample and the reference mirror, respectively. The beams returning from the cell are reflected by a hollow cube corner prism (HCCP) and again introduced into the cell. The paths of A* and B* are reflections of those of A and B, respectively. The four parallel paths are located at respective corners of a square having a size of 10×10 mm on a plane perpendicular to the paths. The two beams returning again from the cell are introduced into another

photodetector (PD2) by a combination of a beam splitter (BS3) and a prism (P2). Beat signals generated by PD2 are measured as probe signals using a lock-in amplifier. Beat signals from PD1 are used as the reference signal. The changes in sample length are determined by comparing the phase of the probe signal with that of the reference signal.

2.3. Vacuum Chamber with Carbon-Composite Heaters

Figure 4 shows a schematic diagram of the experimental setup. All experimental devices have been mounted on a vibration-isolation optical table, except those for data acquisition and analysis. The furnace for heating the sample consisted of carbon-composite heaters and a vacuum chamber whose wall was water-cooled. The chamber was evacuated to 10^{-3} Pa using an oil-free turbo-molecular pump. A dielectric multilayer mirror
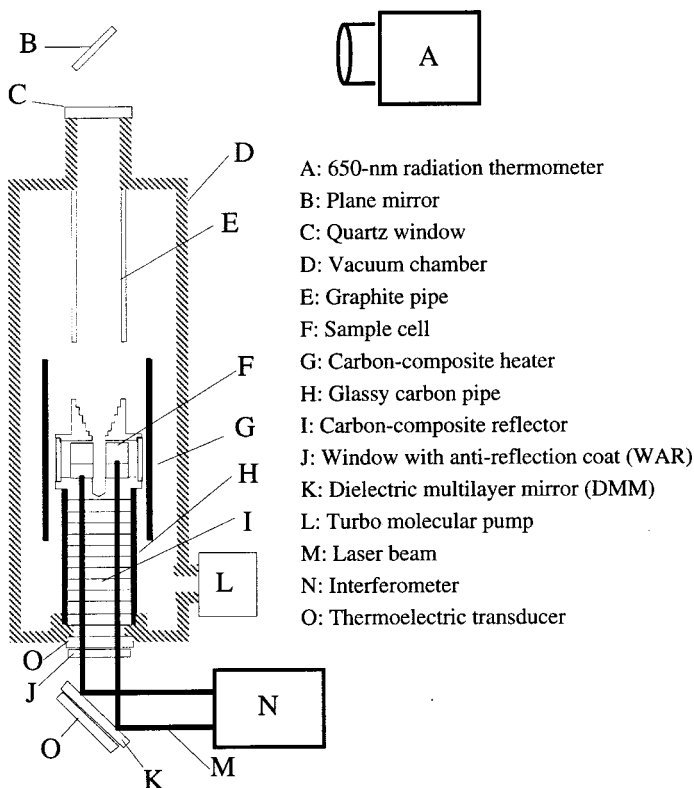

A: 650-nm radiation thermometer
B: Plane mirror
C: Quartz window
D: Vacuum chamber
E: Graphite pipe
F: Sample cell
G: Carbon-composite heater
H: Glassy carbon pipe
I: Carbon-composite reflector
J: Window with anti-reflection coat (WAR)
K: Dielectric multilayer mirror (DMM)
L: Turbo molecular pump
M: Laser beam
N: Interferometer
O: Thermoelectric transducer

Fig. 4. Schematic diagram of the experimental setup.

(DMM) was placed below the bottom end of the chamber, which introduced the laser beams into the chamber. A quartz window with an anti-reflection coat (WAR) was mounted on the bottom end of the chamber, through which the laser beams passed. Temperatures of the DMM and WAR were stabilized using thermoelectric transducers, because the optical components were irradiated by radiation from the sample cell. The reason for stabilizing them is that a change in temperature of the components increases the uncertainty in interferometric measurements.

The tube supporting the cell is made of glassy carbon, having a lower thermal conductivity than that of graphite, to minimize heat losses by thermal conduction from the cell to the chamber wall along the tube. The tube wall was about 1.3 mm thick, which is the lower limit to get sufficient strength. Twenty five carbon-composite discs were piled on top of one another inside the tube, which were used as reflectors against thermal radiation. Each carbon-composite reflector was 2 mm in thickness and had four holes through which the laser beams passed.

2.4. Single Spectral-Band Radiation Thermometer

A single spectral-band radiation thermometer (TOPCON. Co., model: OEP-PM-650ND) was used to measure the temperature of the sample. A silicon photodiode was used as the detector for the pyrometer. The center wavelength of the interference filter was approximately 649.0 nm with a half bandwidth of 17.2 nm. The distance between the sample and pyrometer was about 600 mm, and the target of the pyrometer was a circular area of diameter 1.17 mm. In general, the relation between the radiation temperature (T) and pyrometer signal (V) from the detector is

$$V = \varepsilon_{\mathrm{eff}} C (\exp(c_2/(AT+B)) - 1)^{-1} \tag{1}$$

where A, B, and C are determined by pyrometer calibrations, $\varepsilon_{\mathrm{eff}}$ is the effective target emissivity, and c_2 is the second radiation constant. The values of A, B, and C for the pyrometer were determined by the Thermophysical Metrology Department at the National Research Laboratory of Metrology (NRLM). Based on the calibration for the pyrometer, combined standard uncertainties in the measured values of T are estimated to be 0.95 K at 1500 K, 1.2 K at 1700 K, and 1.4 K at 1900 K.

In the present study, $\varepsilon_{\mathrm{eff}}$ was not identical to $\varepsilon_{\mathrm{cav}}$ for the sample, because there was a quartz window and a plane mirror on the optical path for the pyrometer, which attenuated the intensity of the radiation emerging from the cavity. Therefore, the value of $\varepsilon_{\mathrm{eff}}$ was directly measured by using
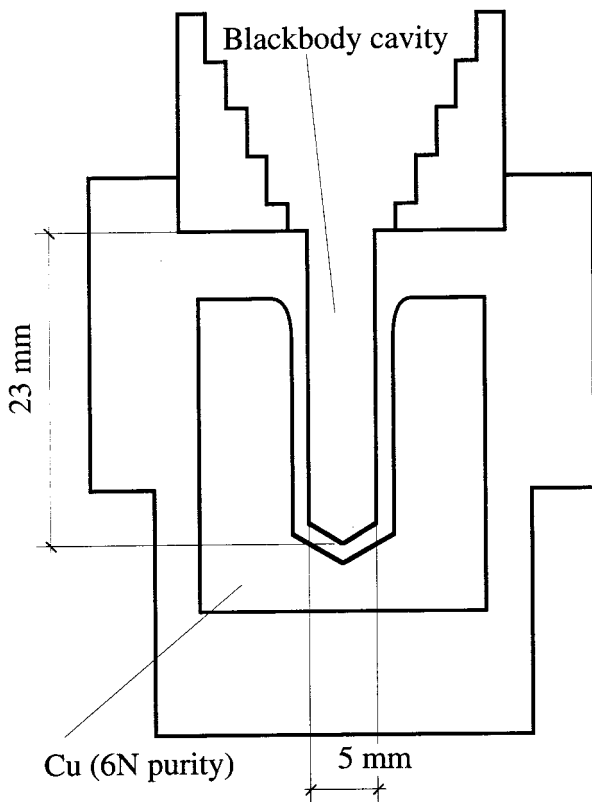
Fig. 5. Schematic diagram of the cross section of the fixed-point blackbody cell.

a fixed-point blackbody as a reference radiation source. Figure 5 shows a schematic diagram of the cross section of the fixed-point blackbody used here. The cylindrical cavity for the blackbody is almost the same as that of the sample in size, and thus its emissivity is estimated as 0.998. The blackbody contained copper of six nines nominal purity by mass as the fixed-point metal and was made from graphite blocks in which the total impurity concentration was lower than 5 ppm by mass. In the measurement of $\varepsilon_{\mathrm{eff}}$, the blackbody replaced the sample cell on the glassy carbon tube, and was first heated to above the Cu melting point (T_{Cu}) in an inert argon atmosphere. After melting the metal completely, the cell was gradually cooled to below T_{Cu}. At that time, a plateau of the output signal from the pyrometer was observed during the solidification of the fixed-point metal. The output signal of V_{Cu} obtained during the plateau corresponds to the intensity of

the blackbody radiation at T_{Cu}. The value of ε_{eff} was estimated to be 0.780 by substituting the measured value for V_{Cu} and nominal value of T_{Cu} into Eq. (1).

2.5. Experimental Procedures

Data on $\alpha(T)$ as a function of the sample temperature (T) have been derived from the following equation,

$$\alpha(T) = \Delta L/(L_{293}\,\Delta T) \tag{2}$$

where ΔT is a given temperature change from T_l to T_h, T is $(T_l + T_h)/2$, L_{293} is the sample length at 293 K, and ΔL is the length change corresponding to ΔT. The measurement was carried out in the following manner. The combination of sample and mirror was set in the sample cell as the optical alignment for the interferometer was optimized. Prior to the measurement, it was heated to 2000 K to eliminate obstacles possibly existing between the sample and mirror and the optical alignment was again adjusted by shifting the DMM and HCCP while the sample temperature was kept constant at 1300 K. The pyrometer and blackbody aperture were also aligned at 1300 K. Output signals from the devices were recorded at regular intervals of 5 s while the sample temperature rose to 2000 K from 1300 K at a rate of about 6.7×10^{-2} K · s⁻¹. In order to measure ΔL and ΔT under steady-state conditions, the temperature was held constant over about 9×10^2 s at a temperature interval of about 100 K on the way to 2000 K from 1300 K. That is, values of $\alpha(T)$ were determined for the condition that ΔT was about 100 K. The dc level of the interferometric signal occasionally decreased under the measurable limit with an increase of temperature because of the deterioration of the alignment. Such weak signals were not taken into the calculations of $\alpha(T)$. The lower limit to be measurable depends upon the magnitude of background noise for the photodetectors used here, which was about 1 mV.

There is a possibility that zero drift in interferometric signals increases as the sample temperature increases, because the drift is caused by a non-uniform temperature field over the optics through which the laser beams pass [6]. Thus, the zero drift was measured four times by using the glassy carbon mirror as a reference. In the measurements, only the mirror was set in the cell, and therefore all four laser beams were reflected by it. An apparent length change corresponding to the drift was determined for a given temperature interval of 100 K.

3. RESULTS AND DISCUSSION

3.1. Measured Values of $\alpha(T)$ for Glassy Carbon

In order to assess the reproducibility of the experimental results, the measurement in the range from 1300 to 2000 K was repeated four times. There are four ways available for setting the sample in the sample cell, because the sample can be placed at two different positions (P1 and P2) in the cell and has two optical flats (F1 and F2). The difference between P1 and P2 is whether the sample reflects the beam for the path A or that for the path B, as shown in Figs. 1 and 3. In ideal conditions, there is no difference among the experimental results obtained under the four settings. However, geometrical conditions of the flats and the configuration of the optical elements in the interferometer are more or less imperfect. Therefore, the sample was relocated or reversed after each measurement run, and, thus, the measurements were carried out under the four settings.

Figure 6 shows the experimental results on $\alpha(T)$ for the measurements with the sample relocation and the curve of the fourth-order polynomial
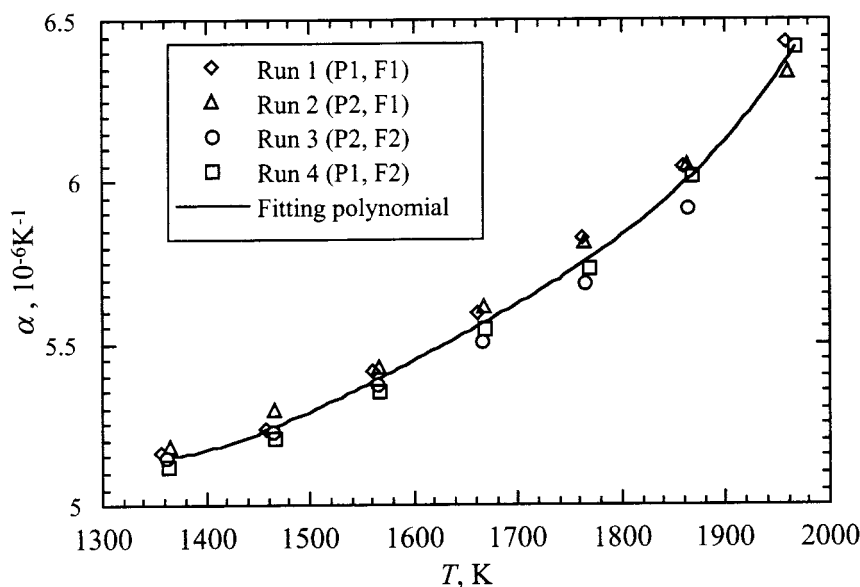

Fig. 6. Experimental results on $\alpha(T)$ for the measurements with the sample relocation, and the curve of the fourth-order polynomial function established by the least-squares fitting routine.

function established by the least-squares fitting routine. The function is given as follows:

$$\alpha(T)/(10^{-6}\text{ K}^{-1}) = 110.69 - 0.26448T + 2.4677 \times 10^{-4}T^2$$
$$- 1.0196 \times 10^{-7}T^3 + 1.584 \times 10^{-11}T^4 \qquad (3)$$

where T is in K. The relative standard deviation of the measured values of $\alpha(T)$ from the values calculated from the fitting polynomial is 0.63%. The four sets of the data show no significant bias towards each other. In run 3, the values of $\alpha(T)$ at temperatures above 1900 K could not be determined because of the decline in the signal intensity under the limit.

3.2. Influence of Sample Relocations on Reproducibility of Experimental Results

In order to check the influence of the sample relocation on the reproducibility of the experimental results, two experimental results with and without sample relocation have been compared. In the measurements without the relocation, a set of $\alpha(T)$ in the range of 1300 to 2000 K was determined five times under the same setting condition. Figure 7 shows the experimental results for $\alpha(T)$ for the measurements without the sample relocation and the curve of the fourth-order polynomial function established by the least-squares fitting routine. The function is given as follows:

$$\alpha(T)/(10^{-6}\text{ K}^{-1}) = 116.89 - 0.27909T + 2.5965 \times 10^{-4}T^2$$
$$- 1.0703 \times 10^{-7}T^3 + 1.6594 \times 10^{-11}T^4 \qquad (4)$$

where T is in K. The relative standard deviation of the values measured without the relocation from the fitting values is 0.20%. Differences between the calculated values for Eq. (3) and those for Eq. (4) are at most 0.59% over the temperature range investigated, and therefore we consider that the two experimental results are identical. However, it must be emphasized that the relative standard deviation for the measurement with the sample relocation is much larger than that without it. The difference in magnitude of the deviation indicates that the sample relocation greatly reduces the reproducibility of the experimental results.

3.3. Analysis of Uncertainties

The uncertainty in the reported values of $\alpha(T)$ arises from uncertainties in the measured quantities of ΔL, ΔT, and L_{293}. In this study, the
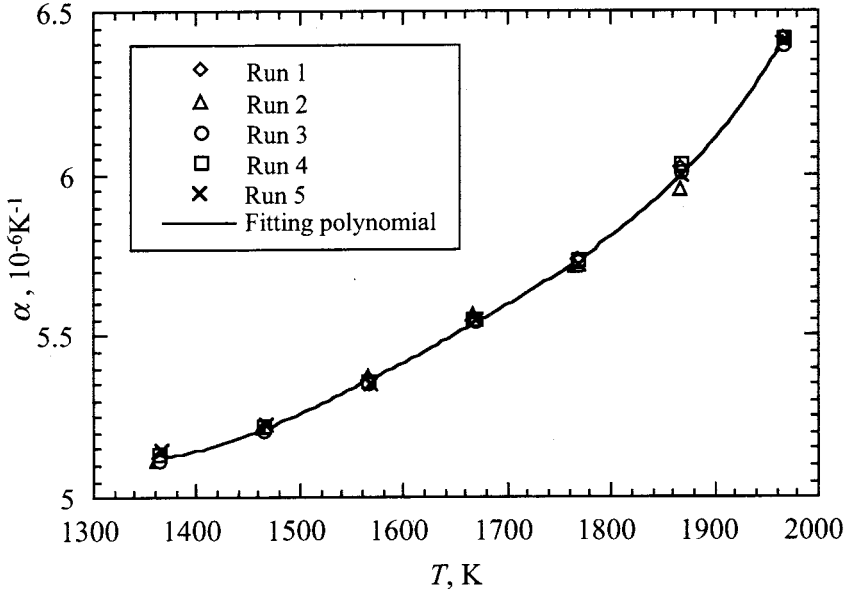
Fig. 7. Experimental results on $\alpha(T)$ for the measurements without the sample relocation, and the curve of the fourth-order polynomial function estimated by the least-squares fitting routine.

combined standard uncertainty ($\Delta\alpha_C$) is estimated by using the following equations,

$$\Delta\alpha_C = \sqrt{(\Delta\alpha_L)^2 + (\Delta\alpha_T)^2 + (\Delta\alpha_{L_{293}})^2}$$

$$\Delta\alpha_L = \frac{\alpha\delta(\Delta L)}{\Delta L}, \qquad \Delta\alpha_T = \frac{\alpha\delta(\Delta T)}{\Delta T}, \qquad \text{and} \qquad \Delta\alpha_{L_{293}} = \frac{\alpha\delta L_{293}}{L_{293}} \tag{5}$$

where $\delta(\Delta L)$, $\delta(\Delta T)$, and δL_{293} are the uncertainties of ΔL, ΔT, and L_{293}, respectively. The sources and magnitudes of uncertainties in the measurements of $\alpha(T)$ are listed in Table I. As a result, the relative values for $\Delta\alpha_C$ are estimated to be 0.86% at 1500 K, 1.3% at 1700 K, and 1.3% at 1900 K. The respective values of 6 mm and 100 K for L_{293} and ΔT are inserted into Eqs. (5) in the estimation of the uncertainties at the three temperatures. In addition, the values of $\alpha(T)$ calculated from Eq. (3) are used for the estimation.

An important finding in the uncertainty analysis is that the contribution of the zero drift to $\Delta\alpha_C$ is predominantly large over the entire temperature

Table I. Sources and Magnitudes of Uncertainties in the Measured Values of $\alpha(T)$ at Three Temperatures

Temperature, T	1500 K		1700 K		1900 K	
α^a	5.29×10^{-6} (K^{-1})		5.62×10^{-6} (K^{-1})		6.12×10^{-6} (K^{-1})	
	Uncertainty^b	$\Delta\alpha$ (K^{-1})	Uncertainty^b	$\Delta\alpha$ (K^{-1})	Uncertainty^b	$\Delta\alpha$ (K^{-1})
$\delta(\Delta L)$						
Zero drift^c	26 nm	4.3×10^{-8}	43 nm	7.2×10^{-8}	46 nm	7.7×10^{-8}
Fringe determination	0.57 nm	9.0×10^{-10}	0.57 nm	9.0×10^{-10}	0.57 nm	9.0×10^{-10}
Laser frequency stability	0.041 nm	6.8×10^{-11}	0.041 nm	6.8×10^{-11}	0.041 nm	6.8×10^{-11}
$\delta(\Delta T)$						
Pyrometer linearity	0.080 K	6.0×10^{-9}	0.14 K	1.1×10^{-8}	0.19 K	1.6×10^{-8}
Reproducibility of the standard radiation source	0.17 K	1.3×10^{-8}	0.21 K	1.7×10^{-8}	0.26 K	2.3×10^{-8}
δL_{293}						
Determination of L_{293}	5 µm	4×10^{-9}	5 µm	4×10^{-9}	5 µm	4×10^{-9}
Combined standard uncertainty,^{d} $\Delta\alpha_C$ (K^{-1})		4.6×10^{-8}		7.5×10^{-8}		8.1×10^{-8}
Relative uncertainty, $(\Delta\alpha_C/\alpha) \times 100$		0.86%		1.3%		1.3%

^{a} Calculated from Eq. (3).

^{b} Estimated under the condition that L_{298} is 6 mm and ΔT is 100 K.

^{c} The magnitude of the apparent length change for the temperature change of 100 K.

^{d} Square root of the sum of the individual uncertainties.

range investigated. This suggests that the uncertainty arising from the sample relocation corresponds to that caused by the zero drift in this study. The zero drift can be related to deviations of the contact between the sample and the mirror and angles between the optical flats and the laser beams from their ideal conditions, as well as to the imperfection of the optical components. Glassy carbon is not easily machined; thus, the parallel optical flats of the sample were not so precisely made as those of other materials. It has been conjectured that such imperfections of the flats enhance the changes in the contact conditions and the angles due to relocating the sample.

Other uncertainties were considered to affect the uncertainty in the values of $\alpha(T)$, but they can be considered as negligible. First, it should be noted that uncertainties caused by systematic effects in T and L hardly contribute to $\delta(\Delta T)$ and $\delta(\Delta L)$ on the assumption that such uncertainties remain almost constant during the interval of 2×10^3 s to produce the temperature change of 100 K. In fact, performances of the pyrometer and the interferometer are extremely stable during such a short period. Therefore, the uncertainty arising from the long-term stability of the pyrometer, which is the main one in the temperature measurements, is not taken into the evaluation for $\Delta\alpha_T$. The uncertainty arising from the inhomogeneous temperature field over the sample is also considered to be negligible. The temperature distribution along the length of the sample was measured by inserting a thermocouple into the combined cavity. As a result, the maximum temperature difference within the sample was about 0.24 K at 1500 K. The uncertainty because of the temperature nonuniformity is estimated to be at most 3×10^{-10} K^{-1}, which is negligible when compared with the value of 5.29×10^{-6} K^{-1} for $\alpha(T)$ at 1500 K. In addition, possible uncertainties caused by vapor deposition on the furnace optical windows can be neglected, because no transmittance losses of the windows were detected during or after each series of experiments.

4. CONCLUSIONS

A laser interferometric dilatometer has been developed for absolute measurements of the thermal expansion of solids under steady-state conditions over the temperature range of 1300 to 2000 K. Performance and operational characteristics of the dilatometer have been assessed by measuring $\alpha(T)$ for glassy carbon. The effect of sample relocation on the reproducibility of the experimental results has been evaluated by comparing relative standard deviations of the reported values of $\alpha(T)$ for measurements with and without the sample relocation.

ACKNOWLEDGMENT

REFERENCES

1. National Bureau of Standards Certificate (Washington, D.C., 1976).
2. T. A. Hahn, Thermal Expansion 6 (Plenum Press, New York, 1978), pp. 191–201.
3. A. Schauer, *Can. J. Phys.* **43**:523 (1965).
4. A. N. Amatuni, T. I. Malyutina, V. Ya. Chekhovskoi, and V. A. Petukhov, *High Temp. High Press.* **8**:565 (1976).
5. A. P. Miiller and A. Cezairliyan, *Int. J. Thermophys.* **3**:259 (1982).
6. A. P. Miiller and A. Cezairliyan, *Int. J. Thermophys.* **6**:695 (1985).
7. A. P. Miiller and A. Cezairliyan, *Int. J. Thermophys.* **11**:619 (1990).
8. M. Okaji and H. Imai, *J. Phys. E* **20**:887 (1987).
9. M. Okaji, *Int. J. Thermophys.* **9**:1101 (1988).
10. M. Okaji, K. Nara, H. Kato, K. Michishita, and Y. Kubo, *Cryogenics* **34**:163 (1994).
11. M. Okaji and N. Yamada, *High Temp. High Press.* **29**:89 (1997).
12. M. Okaji, N. Yamada, H. Kato, and K. Nara, *Cryogenics* **37**:251 (1997).
13. N. Yamada, K. Nara, M. Okaji, T. Hikata, T. Kaneko, and N. Sadakata, *Cryogenics* **38**:397 (1998).
14. M. Okaji, N. Yamada, and H. Moriyama, *Metrologia* **37**:165 (2000).
15. S. Otani and A. Oya, in *Material Science and Technology*, Vol. 9, J. Zarzycki, ed. (VCH-Wiley, Weinheim, 1991), pp. 549–572.
16. J. O. Hylton and R. L. Reid, *AIAA J.* **14**:1303 (1976).
17. R. E. Bedford, in *Theory and Practice of Radiation Thermometry*, D. P. DeWitt and G. D. Nutter, eds. (John Wiley, New York, 1988), p. 653.